Hindawi Publishing Corporation
International Journal of Photoenergy
Volume 2015, Article ID 501978, 12 pages
http://dx.doi.org/10.1155/2015/501978

Research Article

Morphological Effect of CNT/TiO_2 Nanocomposite Photoelectrodes Dye-Sensitized Solar Cell on Photovoltaic Performance with Various Annealing Temperatures

Mohd Zikri Razali,[1] Huda Abdullah,[1] and Izamarlina Asaahari[2]

[1] *Department of Electrical, Electronic & System Engineering, Faculty of Engineering and Built Environment, Universiti Kebangsaan Malaysia, 43600 Bangi, Selangor, Malaysia*
[2] *Fundamental Studies of Engineering Unit (UPAK), Faculty of Engineering and Built Environment, Universiti Kebangsaan Malaysia, 43600 Bangi, Selangor, Malaysia*

Correspondence should be addressed to Huda Abdullah; huda@eng.ukm.my

Received 13 May 2014; Accepted 23 July 2014

Academic Editor: Tao Xu

This research focused on the fabrication of dye-sensitized solar cell based on a photoanode of carbon nanotube/titanium dioxide (CNT/TiO_2) nanocomposite photoanode synthesized through acid-catalyzed sol-gel method. The results show the improvement of the chemical and electrical properties of the solar cells annealed at different temperatures. The CNT/TiO_2 colloidal solution was synthesized using titanium tetraisopropoxide and CNT/2-propanol solution. The thin films were doctor-bladed on a fluorine tin oxide glass before being annealed at 550, 650, and 750°C. The field emission scanning electron microscopy morphological images show that the thin films were homogenously distributed and maintained their spherical structures. The X-ray diffraction patterns show that the films consisted of anatase and rutile phases with large crystallite sizes due to temperature increment. The atomic force microscopy analysis presents the thin film roughness in terms of root mean square roughness. The photovoltaic performance was analyzed using *IV* curve and electrochemical impedance spectroscopy (EIS). The thin films annealed at 750°C had the highest energy conversion efficiency at 5.23%. The EIS analysis estimated the values of the effective electron lifetime (τ_{eff}), effective electron diffusion coefficient, effective electron diffusion (L_n), and effective recombination rate constant (k_{eff}). A large τ_{eff}, small k_{eff}, and longer L_n can improve photovoltaic performance efficiency.

1. Introduction

Dye-sensitized solar cell (DSSC) is considered a relatively new type of solar cell as it was first discovered by O'Regan and Grätzel in 1991 [1, 2]. DSSCs show better potential compared with Si solar cells because they are cheap [3, 4], more environmentally friendly, and simpler to manufacture [5]. DSSCs have attracted substantial attention worldwide. Grätzel's cell has a solar conversion efficiency of ~13%, which is significantly lower than that of Si solar cells. To improve the performance of DSSC devices, a number of factors need to be considered. Electron transport across a TiO_2 electrode is one of the most important factors affecting the conversion efficiency of DSSC. As the electron mobility increases, the DSSC efficiency also increases. However, charge recombination generally inhibits the transport of the injected electrons from TiO_2 to the conducting glass substrate, thus decreasing the performance of DSSCs. Therefore, a rapid photoinduced electron transport in the TiO_2 working electrode and the suppression of charge recombination ensure a higher DSSC conversion efficiency.

A similar literature suggests that carbon nanotubes (CNTs) are suitable semiconductor supports because of their combination of electronic, adsorption, mechanical, and thermal properties [6, 7]. CNTs provide interpenetrating electrodes with high surface areas for DSSCs. The introduction of CNTs into the electrodes of organic solar cells [8, 9] and dye-sensitized solar cells [10] has been performed, and researchers have concluded that CNTs efficiently enhance the electronic conductivity of the electrode, thus increasing the photoconversion efficiency of the photovoltaic device. Furthermore, previous studies have shown that the

introduction of CNTs decreases TiO_2 crystalline grain and particle sizes [11]. Previous studies also suggest that a TiO_2 semiconductor with large particle or crystalline sizes has a large surface area and has numerous contact points among the particles, carbon nanotubes, and underlying substrates. These results are beneficial for the improvement of the cell performance. Therefore, CNTs are regarded as promising materials for use in DSSCs, and the utilization of CNTs to improve the photoconversion efficiency of DSSCs is expected and should be conducted. In the past decade, several studies have reported that the incorporation of CNTs in a nanocrystalline TiO_2 working electrode prepared using blended fabrication with commercial TiO_2 (P25) increases the solar energy conversion efficiency of DSSCs [12]. However, further increasing the CNT loading may inhibit the improvement of DSSC cell performance because of serious CNT aggregations.

In this study, we prepared CNT/TiO_2 nanocomposite thin films annealed at various temperatures from 550°C to 750°C. We investigated the morphological and photocatalytic activity properties of the CNT/TiO_2 solar cell. This morphological structure was examined using field emission scanning electron microscopy (FESEM), X-ray diffraction (XRD), and atomic force microscopy (AFM). The photovoltaic properties of the solar cell were determined using *IV* curve analysis and electrochemical impedance spectroscopy (EIS). The results show that the annealing temperatures significantly affect the combination of TiO_2 nanoparticles with CNT and hence influence the performance of the CNT/TiO_2 dye-sensitized solar cell.

2. Methodology

2.1. Preparation of the CNT/TiO_2 Nanocomposite Solution. The CNT/TiO_2 nanocomposite photoanode was synthesized using modified acid-catalyzed sol-gel method. CNT powder was acid-treated first before being used. The synthesis was conducted by boiling raw CNT in a concentrated nitric acid solution for 5 h. The CNT solution was then filtered and washed with distilled water several times to remove the excess acid. Afterward, the mixture was dried in oven for 24 h. Then, 2-propanol (Solaronix, SA) anhydrate solution (40 mL) was used as the starting material. Precisely 0.06 g of CNT nanopowder (Sigma-Aldrich, USA) was sonicated in the 2-propanol solution for 1 h to adequately disperse the particles. Titanium tetraisopropoxide (TTIP) (10 mL) (Sigma-Aldrich, Belgium), which was the titanium precursor, was poured into the CNT/2-propanol solution. The mixture was continuously sonicated for an additional 1 h to improve the interactions between the two materials. Diluted ethanol (100 mL) was slowly dropped into the solution, and the solution was heated at 100°C for 12 h in a wet furnace to remove the excess water. Last, the CNT/TiO_2 gel-look solution was produced. Figure 1 shows the flowchart of this preparation.

2.2. Preparation of CNT/TiO_2 Nanocomposite Thin Film. Fluorine tin oxide (FTO) glass (Solaronix, SA) was used as the conductive substrate. The FTO glass was ultrasonically cleaned with acetone, methanol, and deionized distilled water. The CNT/TiO_2 thin films were prepared by applying the nanocomposite on the FTO conducting glass. The gel-look product from the above preparation was then added with carbowax 400 (R&M Chemical, UK) that acted as binder. The gel solution was vigorously stirred for 1 h to produce a viscous gel paste. The CNT/TiO_2 nanocomposite mixture was doctor-bladed onto the conductive substrate to form a 0.25 cm^2 active area. The thin films were dried on a hot plate at 60°C for 15 min. Subsequently, the CNT/TiO_2 thin films were annealed in air using a dry furnace at different annealing temperatures of 550, 650, and 750°C for 30 min. Figure 2 shows the flowchart of this preparation.

2.3. Preparation of CNT/TiO_2 Dye-Sensitized Solar Cell. The fabricated dye-sensitized solar cell has two parts, namely, CNT/TiO_2 thin film electrode and platinum thin film counter electrode. The electrodes were immersed in ruthenium dye (N719-Solaronix, SA) for 24 h. The counter electrodes were coated with platinum thin film using screen printing technique and annealed in a furnace at 350°C for 30 min. A parafilm spacer was sandwiched between the annealed CNT/TiO_2 and counter electrodes, and both sides of the substrate were clipped. Iodolyte MPN-100 (Solaronix SA) was used as the electrolyte in this solar cell. The dye-sensitized solar cell frame was sealed using silicon glue to prevent electrolyte leakage during the experiments. Figure 3 shows the flowchart of this preparation.

2.4. Characterization. The morphological structures and energy-dispersive X-ray (EDX) analysis of the CNT/TiO_2 thin films were analyzed and conducted using a FESEM instrument (Zeisz Supra: 15 kV). XRD analysis was conducted using an X-ray diffractometer (Siemens D-5000) with Cu$K\alpha$ irradiation (λ = 1.5406 Å) to determine the crystalline orientations of the CNT/TiO_2 thin film. AFM analysis was conducted to determine the average roughness of the thin film using 3D images. A G300 instrument (GAMRY Instruments) with simulated AM 1.5 xenon illumination having a 100 mW/cm^2 light output was used to analyze the photovoltaic efficiency and electrochemical impedance of the solar cell.

3. Result and Discussion

3.1. Field Emission Scanning Electron Microscopy (FESEM). Figure 4 shows the FESEM images of the surface morphologies of the CNT/TiO_2nanocomposite thin films sintered at different temperatures. From these FESEM images, we can see the arrangement of CNT particles within the nanoporous CNT/TiO_2 films [13]. The diluted ethanol solution acted as the solvent and as a soft template for the films. This preparation technique generates good interactions between the CNT and TiO_2 nanoparticles. The diluted ethanol also improves the pore formation within the nanocomposite thin films. In addition, acid-catalyzed modification method assists in the formation and interactions between the CNT and TiO_2 nanoparticles because of the strong chemical absorption [14].

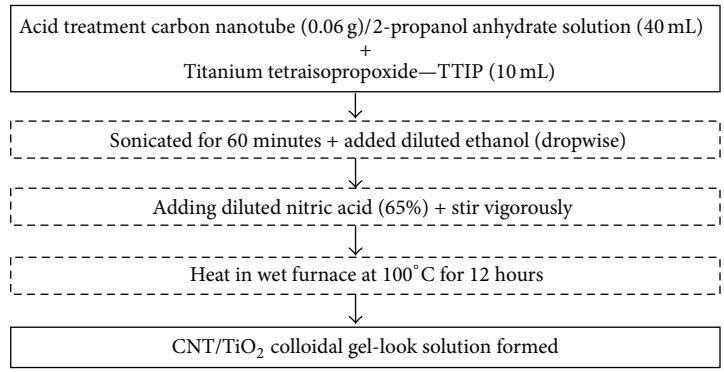

Figure 1: Flowchart for CNT/TiO_2 nanocomposite solution.

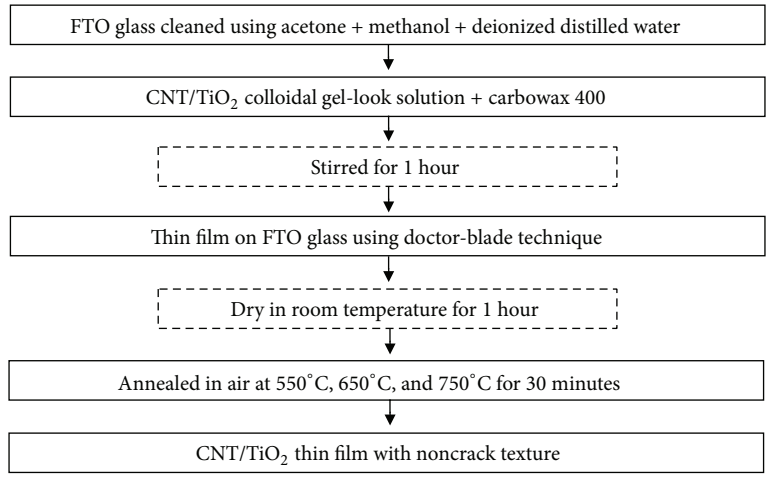

Figure 2: Flowchart for CNT/TiO_2 nanocomposite thin films.

Although this preparation technique limits the crystalline growth of the nanocomposite, it still improves the dye absorption for dye-sensitized solar cell application.

Figure 4 also presents the images of the CNT/TiO_2 thin films annealed at 550, 650, and 750°C. These images were observed at 100 nm with 20 Kx magnifications. All the annealed samples consisted of irregularly arranged and shaped TiO_2 and CNT nanoparticles. The thin film nanoparticles were randomly connected to a noncrack surface. We found that CNT nanoparticles had large sizes in the pore structures of almost all samples, especially for the thin film annealed at 750°C [15]. We also noticed that the varying temperatures affected the morphological structures of the films. The addition of diluted ethanol assisted in the dispersion of the CNT/TiO_2 nanoparticles. Highly dispersed films, in turn, assisted the electron transport inside the films. The films annealed at high temperatures generated large particles size of around 10 nm to 20 nm and produce large surface areas with high porosities inside the films for dye absorption. Another researcher [16] confirmed that samples annealed at high temperatures show more sintered nanoparticles that merged to form the neck between adjacent nanoparticles with better contacts for efficient electron transfer.

Figure 5 shows the average thickness of all samples. Table 1 shows that the average thicknesses for samples annealed at 550, 650, and 750°C were approximately 21.68, 21.27, and 16.07 μm, respectively. High annealing temperatures decrease the average thickness because of the resulting large surface areas and high porosities inside the films. Table 1 presents the data for EDX analysis conducted from the FESEM analysis. The EDX analysis was used to identify the elements or materials contained in the thin films. Figure 6 shows the EDX data to simplify it using a graphical diagram. From this analysis, we discovered the presence of carbon (C), titanium (Ti), and oxygen (O) in all samples. The carbon and titanium elements almost linearly increased with increasing annealing temperature as mentioned in another study [17]. Besides EDX measurement, all these elements (C, Ti, and O) can be proven and supported by using the X-ray diffraction (XRD) measurement analysis.

3.2. X-Ray Diffraction (XRD). The phase transition of the CNT/TiO_2 thin films was studied based on the annealing temperatures. Figure 7 shows the XRD patterns of the CNT/TiO_2 thin films annealed at 550, 650, and 750°C,

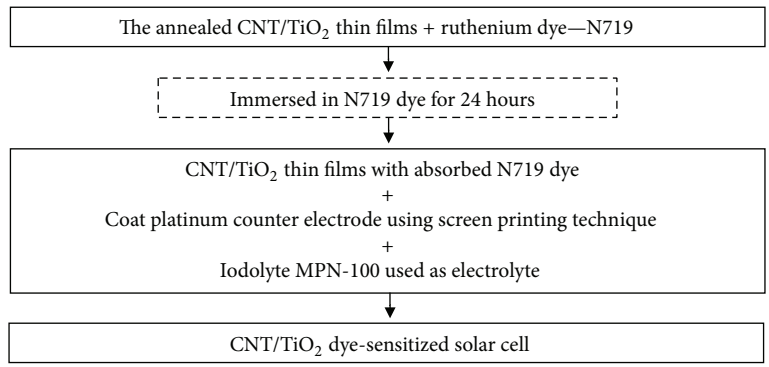

Figure 3: Flowchart for CNT/TiO_2 dye-sensitized solar cell fabrication.

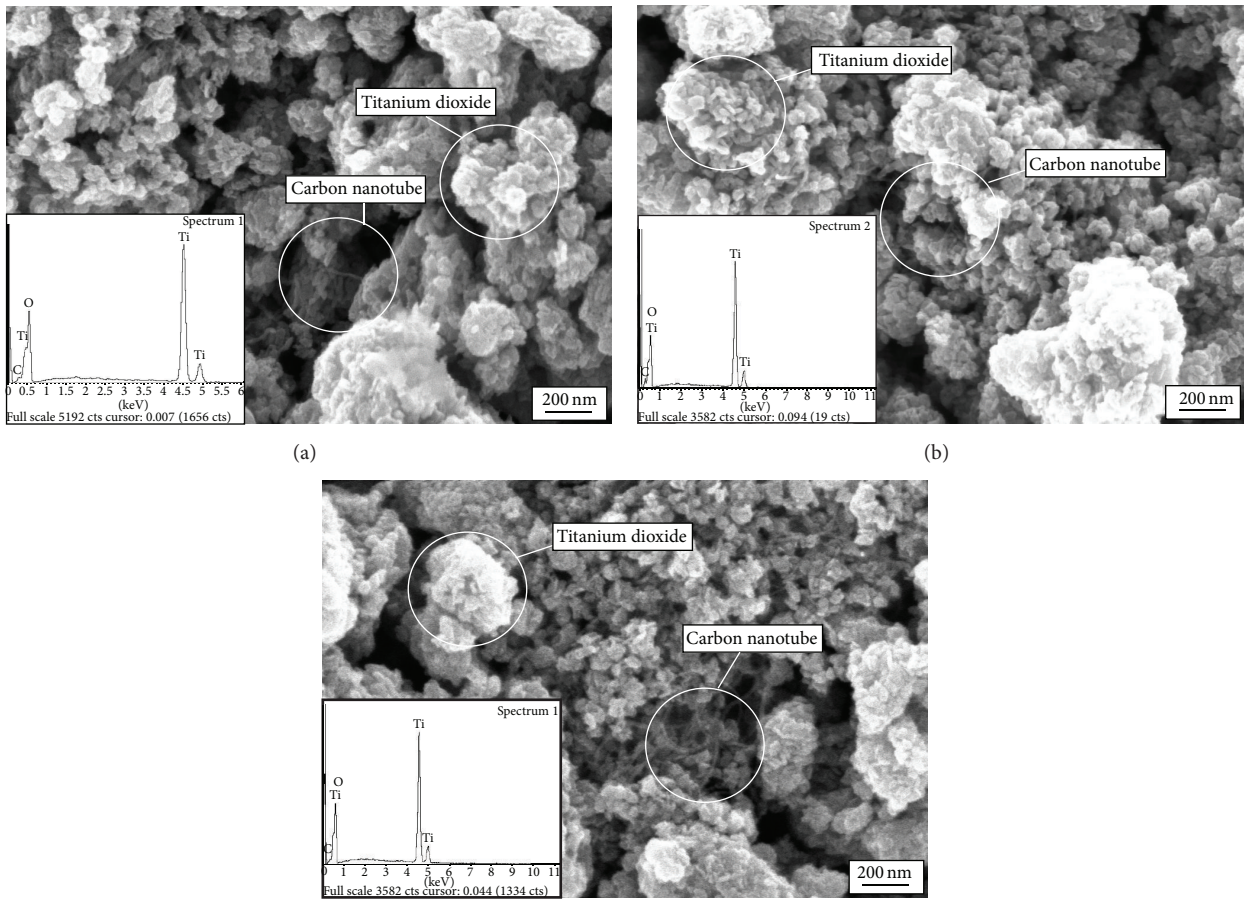

Figure 4: FESEM images of CNT/TiO_2 thin films annealed at different temperatures: (a) 550°C, (b) 650°C, and (c) 750°C.

respectively. As the annealing temperature increases, the TiO_2 nanoparticles go through phase transitions to achieve anatase and rutile structures. The patterns were analyzed and compared using the database file of PDF number 01-078-2486 (TiO_2-anatase) and PDF number 01-086-0147 (TiO_2-rutile). The XRD patterns were calculated at an angle of 2θ between 20° and 60°. The peaks that appeared from these patterns were (101), (004), (200), and (211) at 25.2°, 37.96°, 47.84°, and 55.40°, respectively, for the anatase phase, and the peak was (211) at 54.04° for the rutile phase. The major peaks corresponded to the anatase phase with a crystallographic plane of (101) at 25.2° for all the films. The rutile phase was hardly observed and only occurred in the thin film annealed at 750°C. Brookite phase was not observed in these patterns.

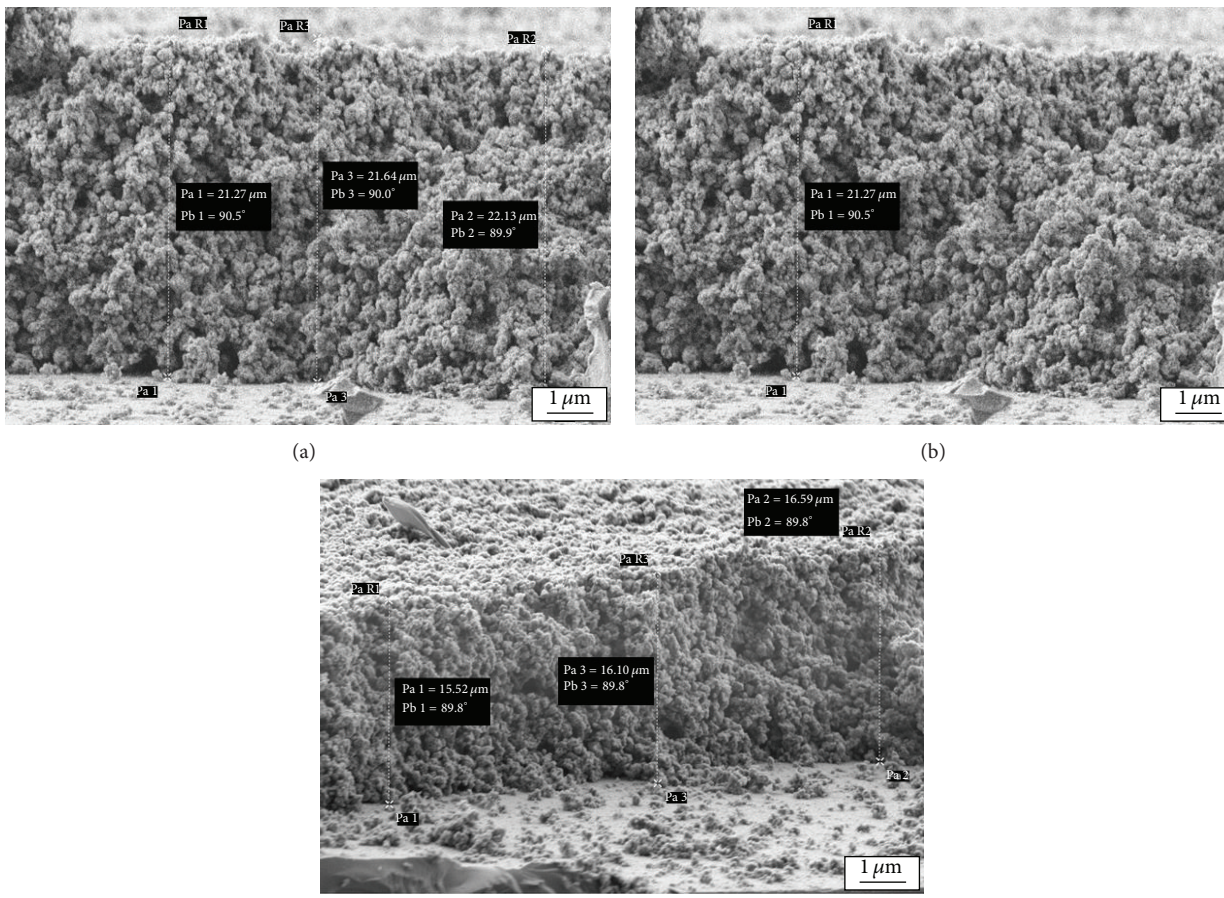

Figure 5: CNT/TiO_2 thin film's average thickness of (a) 550°C, (b) 650°C, and (c) 750°C annealing temperature.

Table 1: EDX analysis data for all CNT/TiO_2 thin films.

Sample	Temperature, °C	Element weight, %		
		Carbon	Titanium	Oxygen
(a)	550	1.31	52.78	45.91
(b)	650	1.42	54.91	43.67
(c)	750	1.46	53.58	44.96

Table 2: XRD analysis parameters for all CNT/TiO_2 thin films.

Sample	Temperature, °C	Major peak	Crystalline size, nm	Lattice parameter		
				a	*b*	*c*
(a)	550	Anatase	15.62	3.7845	Null	9.5143
(b)	650	Anatase	17.10	3.7845	Null	9.5143
(c)	750	Anatase	17.96	3.7845	Null	9.5143

Based on other studies [18, 19], the CNT peaks are usually located at 26.0° and 43.4°, although CNT elements were not detected in this present study. This phenomenon could occur because of the peaks of the crystalline TiO_2 anatase phase at 25.2°, which partly covers the CNT main peak at 26.0°. Moreover, overlapping peaks may occur because the crystalline structure of TiO_2 is larger than that of CNT. A quantitative evaluation of the crystallite size using Scherrer's equation was conducted and the results are shown in Table 2 with a graphical diagram in Figure 8:

$$D = \frac{k\lambda}{B\cos\theta}, \tag{1}$$

where λ is the wavelength of 1.492 nm, B is the full width at half-maximum of the main peak, and θ is the main peak position divided by 2 [20, 21]. Scherrer's equation proves that the film crystallite size slightly increased with increasing of annealing temperatures. The data in Table 2 show that the crystallite sizes for the thin films annealed at 550, 650, and 750°C are 15.62, 17.10, and 17.96 nm, respectively.

The crystallite size increased, and the crystal size in the nanoparticles grew with increasing temperature. The comparison with the XRD peaks of P25, which contains both anatase and rutile phases, confirmed that the annealed TiO_2 nanoparticles at 750°C formed rutile peaks. In high-temperature annealing, the average crystal size increases, reducing the grain boundaries and crystal defects because of the present anatase and rutile phases. The decreased number of trap sites on the nanoparticles reduced the number of

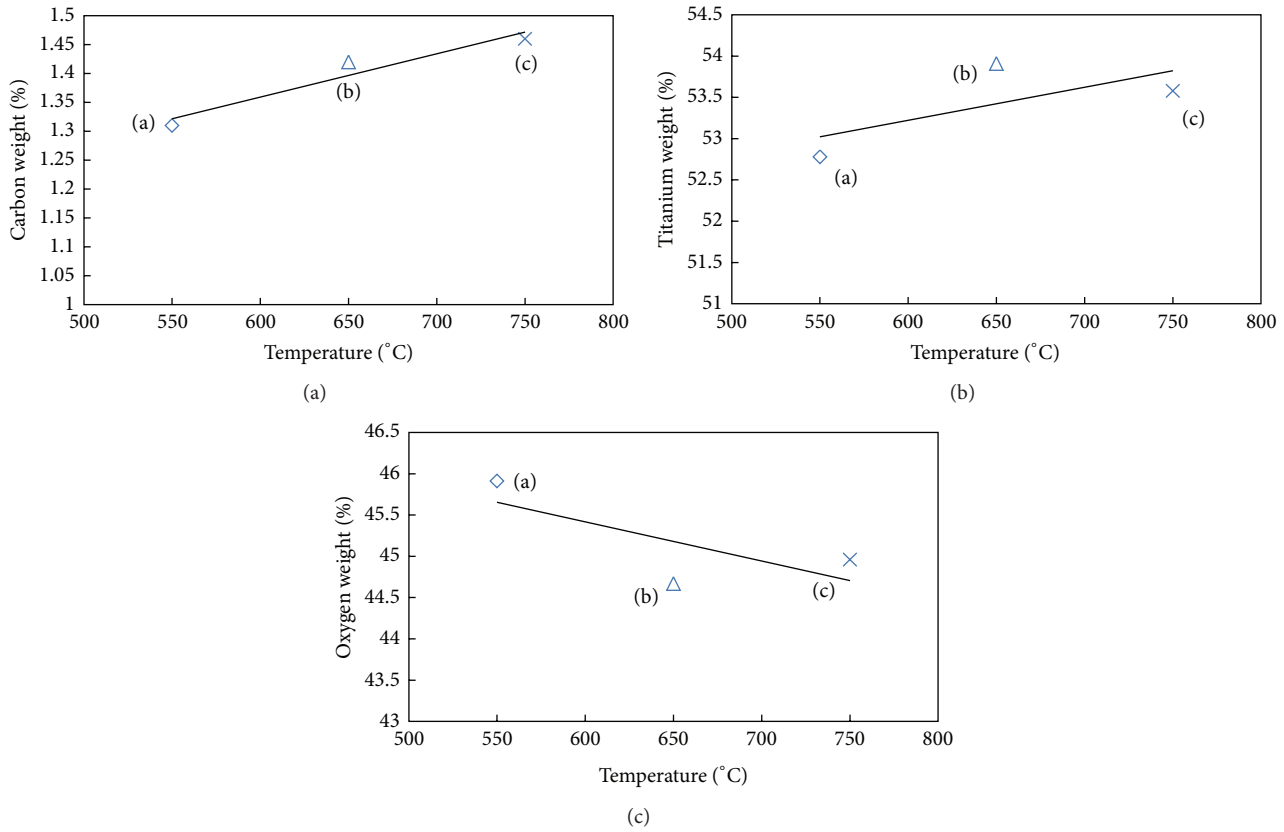

Figure 6: EDX graphical data for (a) carbon, (b) titanium, and (c) oxygen versus annealing temperature.

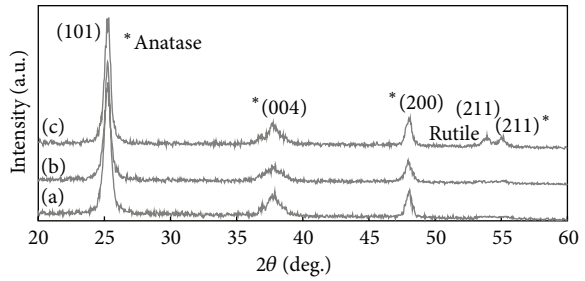

Figure 7: XRD patterns of CNT/TiO_2 films annealed at (a) 550°C, (b) 650°C, and (c) 750°C.

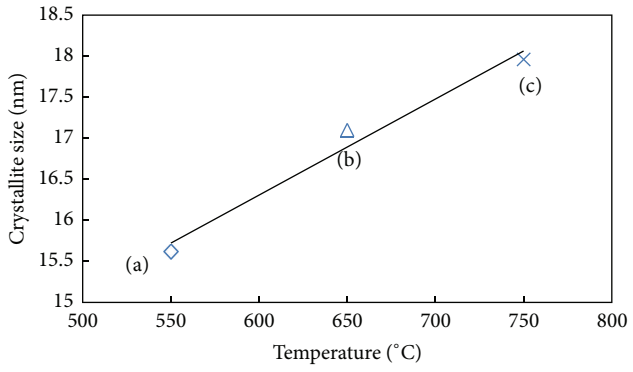

Figure 8: XRD graphical data for crystallite size versus temperature.

obstacles for the fast-moving electron. These effects influenced the charge-trap conditions and consequently increased the electron diffusion speed [22]. Although the combination of the anatase and rutile phases has been proven to enhance the photocurrent density, excessive rutile TiO_2 nanoparticles could form a barrier for the electrons because of high-energy level of the rutile phase [23]. Therefore, the best and optimum temperature determined in this present study is 750°C because the sample annealed at this temperature provided a combination of small amounts of the rutile and anatase phases.

The increase in crystallite size of the TiO_2 nanoparticles provides a better contact point between the nanoparticles. Hence, this advantage provides a more efficient charge transport and faster photo induction for the electron transfer [24]. The lattice parameter data in Table 2 from the database PDF number 01-078-2486 (TiO_2-anatase) show the same value for all the samples with $a = 3.7845$, $b =$ null, and $c = 9.5143$. These results suggest that the incorporation of CNTs into TiO_2 thin films does not affect the TiO_2 lattice structure [25].

3.3. Atomic Force Microscopy (AFM). The CNT/TiO_2 thin film topography and upper surface were observed using AFM. The images in Figure 9 show the samples from all annealing temperatures. These images show that, with increasing annealing temperature, the texture of the thin films becomes rougher and the nanoparticle arrangement becomes

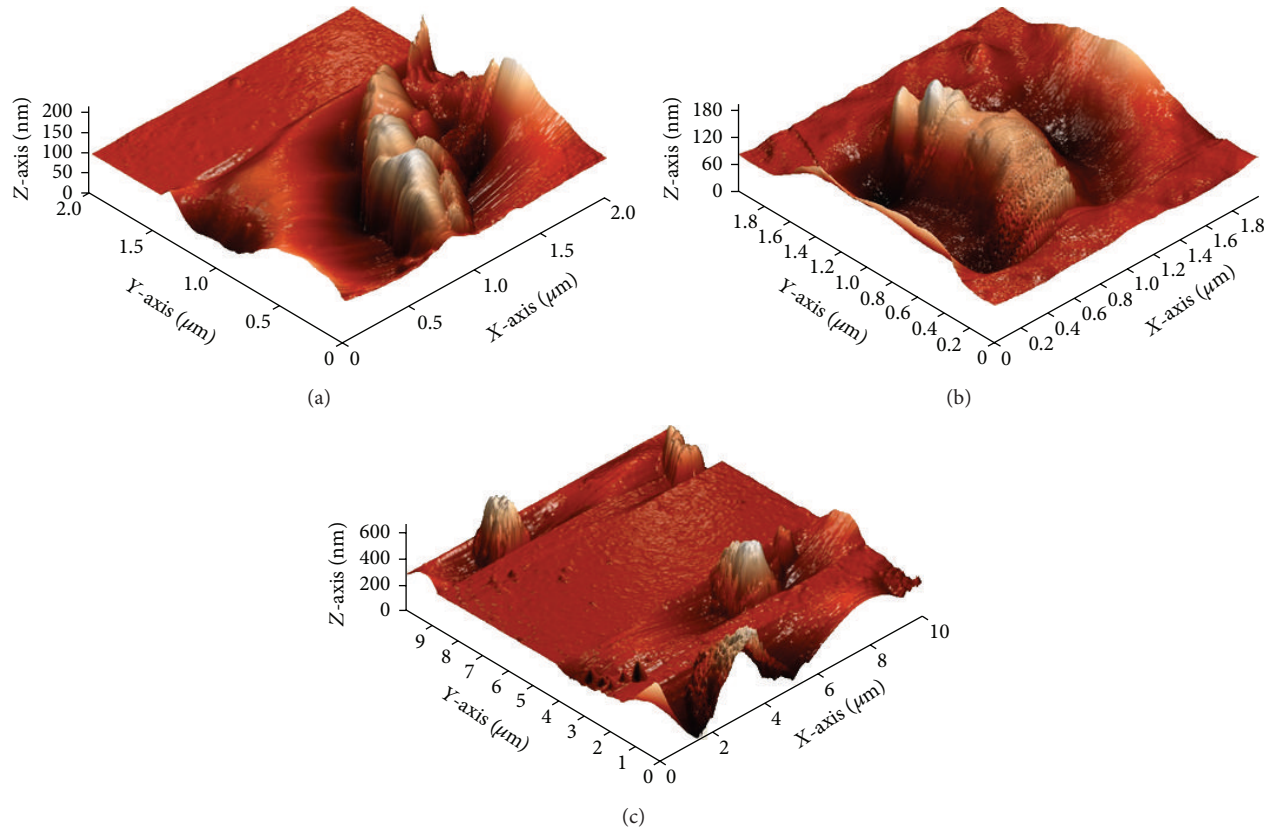

Figure 9: AFM images for CNT/TiO_2 films annealed at (a) 550°C, (b) 650°C, and (c) 750°C.

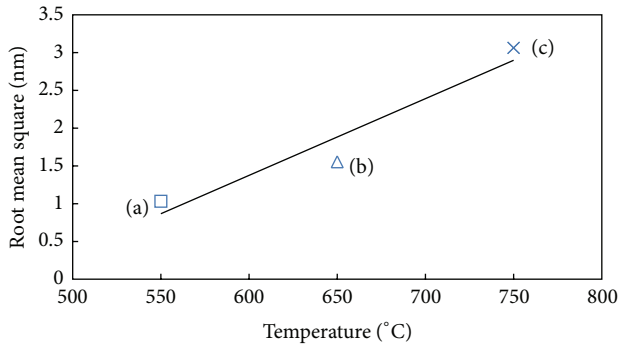

Figure 10: Graph for roughness average versus annealing temperature.

structured. The root mean square roughness (R_q) values demonstrate the morphologies of the films with a uniform and dense granular surface structure. The AFM results confirm that the lowest annealing temperature (550°C) has R_q value of only around 1.032 nm. The roughness average gradually increases with increasing annealing temperature. Average roughness values for thin films annealed at 650°C and 750°C are 1.554 nm and 3.063 nm, respectively. The R_q values for all films are listed in Table 3 and are graphically shown in Figure 10.

Table 3: Root mean square roughness (R_q) data for all samples.

Sample	Temperature, °C	Root mean square roughness (R_q), nm
(a)	550	1.032
(b)	650	1.554
(c)	750	3.063

The AFM measurements analyzed the surface morphologies of the thin films. This characterization is significant to the photoelectrode of the solar cell as the reflection angle of photoelectrode surface can be investigated from R_q values. With the increase in roughness, the increase in the surface texture angle in the thin films will bounce the light on the surface films, indirectly reflecting it back to the film surface. This phenomenon shows that the thin film thickness and crystallite size decrease as the average roughness increases with increasing annealing temperature. This phenomenon can increase the light absorption of the photovoltaic metal oxide and improve the light-to-electricity conversion energy because the light or photon reflectance angle decreased [26].

3.4. Dye-Sensitized Solar Cell Efficiency Performance. Figure 11 shows the *IV* curves of the CNT/TiO_2 dye-sensitized solar cell. The efficiency of the photoelectric conversion

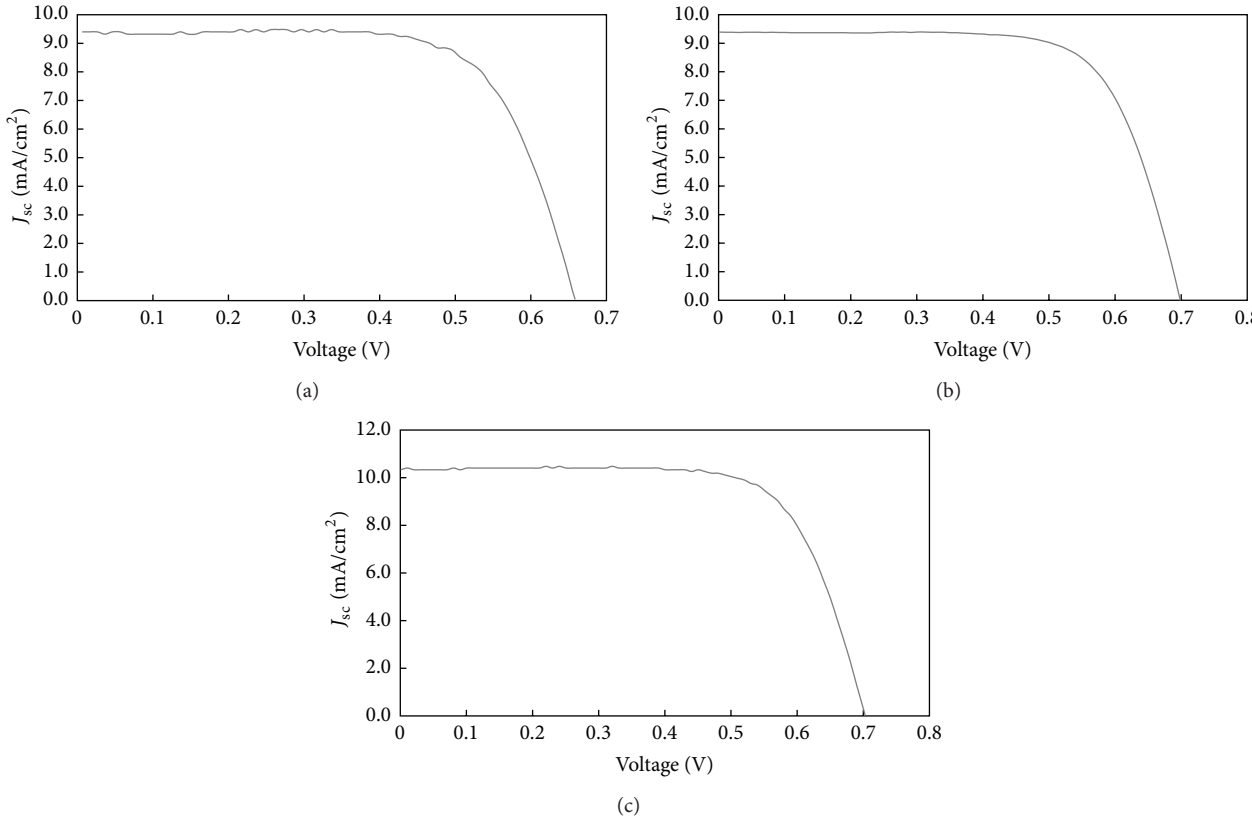

Figure 11: I-V curve efficiency for dye-sensitized solar cell annealed at (a) 550°C, (b) 650°C, and (c) 750°C.

of the photoelectrode solar cell is strongly dependent on the annealing temperature and concentration of added CNT. The active areas of solar cell photoelectrode were around 0.25 cm^2 [27]. The maximum current or short-circuit current density (J_{sc}) (mA/cm^2) was obtained when the solar cell was short-circuited. The open-circuit voltage (V_{oc}) (V) was determined from the potential difference between the CNT/TiO_2 conduction band edge and electrochemical potential of the redox couple of the electrolyte. The fill factor (FF) and solar energy conversion efficiency (η) can be determined using equations [28, 29]

$$\begin{aligned} \mathrm{FF} &= \frac{I_{\max} \times V_{\max}}{I_{sc} \times V_{oc}}, \\ \eta &= \frac{P_{out}}{P_{in}} \times 100 = \frac{I_{\max} \times V_{\max}}{P_{in}} \times 100 \\ &= \frac{I_{sc} \times V_{oc} \times \mathrm{FF}}{P_{in}} \times 100. \end{aligned} \tag{2}$$

Table 4 shows the evaluated and summarized data from the solar cell efficiency analysis. Both V_{oc} and J_{sc} increased from 0.68 V to 0.71 V for (V_{oc}) and from 9.40 mA/cm^{-2} to 10.33 mA/cm^{-2} for (J_{sc}). The FF and η also increased with increasing the annealing temperature. The FF increased from 69% to 71% for the annealed thin films at 550°C to 750°C. η expectedly increased gradually from 4.53%, 4.67%, and 5.23% for the thin films annealed at 550, 650, and 750°C, respectively.

Figure 12 represents the graphical diagram of the efficiency versus temperature. The increasing annealing temperature and insertion of CNT decrease the internal resistance at the TiO_2/dye/electrolyte interface, thus reducing the charge recombination rate of the excited electrons and holes in the dye-sensitized solar cell [30]. These factors cause the increase in the V_{oc} and J_{sc} values of these solar cells. The improvement in the short-circuit current densities shows the improvement in the collection and transport of electrons between the conductive substrate and thin films in the dye-sensitized solar cell [31]. The highest efficiency was achieved through the morphological structures of the thin films. From FESEM images, we can see that the thin film annealed at 750°C is significantly compact and has high porosity. The thin film also has a compact structure with unagglomerated dispersed nanoparticles that enhances the dye absorption on the TiO_2 surface. Moreover, the thin films consisting of anatase and rutile phases reduce the internal obstacle and assist in the electron transport in the cell. The thin film annealed at 750°C and formed with a high average roughness captures more electrons and reflection of photons from the sun into the photoelectrode area.

However, the CNT concentration should be maintained at ~0.06 g to avoid agglomeration within the films, which causes light-harvesting competition between the dye and

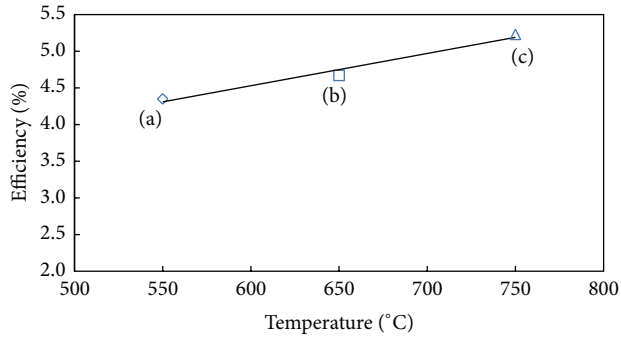

Figure 12: The DSSC percentage efficiency versus temperature for all samples.

Table 4: Dye-sensitized solar cell parameter data for all samples.

Sample	Temperature/°C	V_{oc}/V	J_{sc}/mA/cm^{-2}	Fill factor/%	η/%
(a)	550	0.68	9.40	69	4.35
(b)	650	0.70	9.39	71	4.67
(c)	750	0.71	10.33	71	5.23

CNT that consequently increases the charge transport resistance and reduces the solar cell efficiency [32]. In addition, excess CNT may cause aggregation of the TiO_2 grains (as observed in the FESEM result), resulting in a decrease in amount of adsorbed dye on the working electrode. Moreover, excessive amounts of CNT may cause the working electrode to be less transparent, leading to a reduced DSSC efficiency.

3.5. Electrochemical Impedance Spectroscopy. EIS analysis was used to investigate the electron transport and charge recombination that occurs in these CNT/TiO_2 dye-sensitized solar cells. The solar cell impedance spectrum from EIS analysis is generally composed of three semicircles, which are usually recognized as Z_1: Pt/Electrolyte, Z_2: TiO_2/Dye/Electrolyte, and Z_3: diffusion of I_3^- in the electrolyte. The transmission line for DSSC generally consists of several resistances and capacitances, which are situated in different boundaries. The R_{Pt} and C_{Pt} are the charge-transfer resistance and capacitance in the counter electrode/electrolyte boundary, respectively. The sheet resistance of the conducting substrates, R_s, and charge-transfer resistance, R_{ct}, are attributable to the electron recombination in the electrolyte/CNT/TiO_2/dye boundary. R_t is the electron transport resistance at the metal oxide photoanode, and C_μ is the chemical capacitance within the metal oxide conductive electrode. Z_D is the limited Warburg impedance and redox diffusion in the electrolyte. R_{FTO} and C_{FTO} are the charge-transfer resistance and internal capacitance for the electron recombination in the FTO/electrolyte boundary, respectively. By using the fitted line from the transmission equivalent circuit model, we can plot and analyze the impedance spectra [33].

Figures 13(a) to 13(c) illustrate the DSSC impedance spectrum in the Nyquist plot diagram for the thin films annealed at 550, 650, and 750°C. In Figure 13, the high frequency semicircle Z_1 corresponds to the counter electrode R_{Pt} and Helmholtz C_{Pt}. The middle semicircle indicates the R_{ct} and C_μ between the metal oxide and electrolyte layers of the CNT/TiO_2. The last semicircle at low frequency is attributed to the diffusion impedance in the electrolyte boundary [34]. Although the Nyquist plot diagram in Figures 13(a) to 13(c) does not show three perfect semicircles, the parameters for the solar cell performance still can be extracted from the impedance spectra. The parameters are as follows:

(i) k_{eff} is the reaction rate constant of the electron recombination in the metal oxide interface and is estimated from the peak frequency ω_{max} at the center of the semicircle;

(ii) τ_{eff} is the effective electron lifetime within the solar cell and is calculated from

$$\tau_{eff} = \frac{1}{2\pi f_{max}}; \quad (3)$$

(iii) τ_{eff} is the inverse of k_{eff}, which determines the peak frequency of the CNT/TiO_2 semicircles and is defined as

$$\omega_{max} = f_{max} = k_{eff} = \frac{1}{\tau_{eff}}; \quad (4)$$

(iv) D_{eff} is the effective electron diffusion coefficient and calculated as

$$D_{eff} = \left(\frac{R_{ct}}{R_t}\right)\left(\frac{L^2}{\tau_{eff}}\right), \quad (5)$$

where L is the photoanode thin film thickness and R_{ct} and R_t are estimated from the EIS measurement;

(v) L_n is the effective electron diffusion length of the CNT/TiO_2 photoelectrode and is determined as

$$L_n = D_{eff} \times \tau_{eff}. \quad (6)$$

Figure 13 and Table 5 demonstrate all the three CNT/TiO_2 photoelectrode solar cell diagrams and the data from the different film thicknesses and annealing temperatures. Several differences are observed and these can assist us to determine the solar cell internal performance (e.g., D_{eff} and τ_{eff} data). Even though the thin film annealed at 550°C has significantly higher D_{eff} (8.37×10^7 cm^{2}s^{-1}) compared with the other samples, it has the lowest τ_{eff} (14.33 ms). The thin films annealed at 650°C and 750°C have significantly higher τ_{eff} values (27.01 ms and 100.35 ms, resp.). The k_{eff} for the thin film annealed at 750°C is the lowest. These circumstances decrease the electron transport rate within the cell and consequently affect the overall solar cell performance. From the photovoltaic measurements, we determined the solar cell efficiency to be around 5.23% for the thin film annealed at 750°C, and this result is supported and proven by the EIS analysis. EIS analysis results show that the thin film has τ_{eff} = 100.35 ms, k_{eff} = 9.96×10^{-3}, D_{eff} = 1.76×10^7,

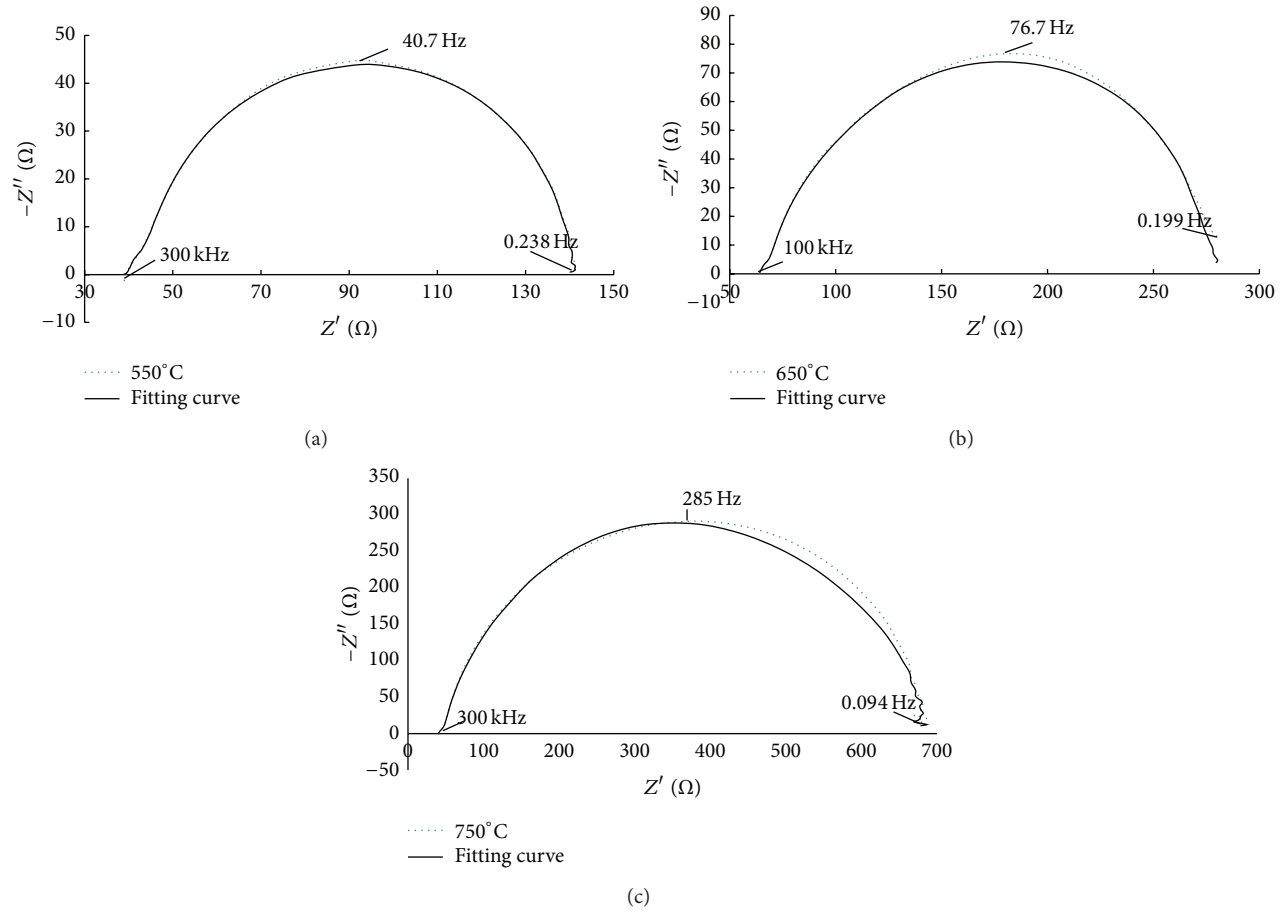

Figure 13: Electrochemical impedance spectroscopy (EIS) measurements for (a) 550°C, (b) 650°C, and (c) 750°C.

Table 5: Parameters determined by electrochemical impedance spectroscopy analysis.

Sample	L (μm)	ω_{max} (Hz)	R_s (Ω)	R_{ct} (Ω)	R_t (Ω)	R_{Pt} (Ω)	C_μ (μF)	Z_D	τ_{eff} (ms)	K_{eff} (s^{-1})	D_{eff} ($cm^2 \cdot s^{-1}$)	L_n (μm)
(a)	21.68	40.7	31.12	7.35	2.88×10^{-6}	9.68	2.79×10^{-5}	0.052	14.33	6.98×10^{-2}	8.37×10^{7}	1.20×10^{9}
(b)	21.27	76.7	34.56	8.43	2.82×10^{-6}	10.64	2.81×10^{-5}	0.054	27.01	3.70×10^{-2}	5.01×10^{7}	1.35×10^{9}
(c)	16.07	285	37.83	20.66	3.02×10^{-6}	12.86	3.34×10^{-5}	0.060	100.35	9.96×10^{-3}	1.76×10^{7}	1.77×10^{9}

and $L_n = 1.77 \times 10^9$. These improvements are caused by the increasing annealing temperature that improves and enhances the surface morphology and thin film thickness of the solar cell. Moreover, the L_n of the thin film is larger compared with its film thickness (16.07 μm), which is important for a high efficiency [35, 36]. A high annealing temperature also has a positive effect as the thin film annealed at 750°C has a large surface area for dye adsorption and high porosity that assist in the electron transport inside the films. Based on a previous study [37], the recombination effects in a photoelectrode from the back reaction, low catalytic activity in counter electrode (redox couple decrease), and slow electron/ion transport between the photoelectrode and counter electrode are the main limitations of a dye-sensitized solar cell.

4. Conclusion

In conclusion, dye-sensitized solar cells based on CNT/TiO_2 photoelectrode were successfully fabricated. The solar cell preparation with different annealing temperatures (550, 650, and 750°C) has a high power conversion efficiency. Precisely 0.06 g of CNT was used in this research. We confirmed that the CNT/TiO_2 solar cell annealed at 750°C provides the highest photoconversion efficiency (5.23%) compared with those annealed at 550°C and 650°C (4.35% and 4.67%, resp.). The FESEM and XRD analysis results show that the thin films are compact and noncrack and have high porosities. The best annealing temperature is 750°C as the anatase and rutile phases occur within the film formed at this temperature. The combination improves the electron mobility within the cell.

AFM analysis shows that the roughness average of the film is 31.063 nm. In EIS analysis, thin film annealed at 750°C has better τ_{eff} (100.35 ms), which improves the electron transport within the cell and reduces the recombination reaction rate by almost 75% compared with other solar cells. The excellent electron transport was also determined from $D_{\text{eff}} = 1.76\times10^{7}$, effective $k_{\text{eff}} = 9.96 \times 10^{-3}$, and $L_n = 1.77 \times 10^{9}$. All these measurements and analyses proved that the dye-sensitized solar cell annealed at 750°C has the best morphological and internal structure to achieve high photovoltaic efficiency.

Conflict of Interests

The authors declare that there is no conflict of interests regarding the publication of this paper.

Acknowledgments

The authors are grateful to the Laboratory of Photonics Institute of Microengineering and Nanoelectronics (IMEN) and Centre for Research and Instrumentation Management (CRIM), Universiti Kebangsaan Malaysia, for providing the facilities. The work was partially supported by a Grant from the Ministry of Higher Education (ERGS/1/2013/TK07/UKM/03/2).

References

[1] B. O'Regan and M. Grätzel, "A low-cost, high-efficiency solar cell based on dye-sensitized colloidal TiO_2 films," *Nature*, vol. 353, no. 6346, article 737, 1991.

[2] M. Grätzel, "Photoelectrochemical cells," *Nature*, vol. 414, no. 6861, pp. 338–344, 2001.

[3] Q. Zhang, C. S. Dandeneau, X. Zhou, and C. Cao, "ZnO nanostructures for dye-sensitized solar cells," *Advanced Materials*, vol. 21, no. 41, pp. 4087–4108, 2009.

[4] M. Grätzel, "Perspectives for dye-sensitized nanocrystalline solar cells," *Progress in Photovoltaics: Research and Applications*, vol. 8, no. 1, pp. 171–185, 2000.

[5] J. van de Lagemaat, N.-G. Park, and A. J. Frank, "Influence of electrical potential distribution, charge transport, and recombination on the photopotential and photocurrent conversion efficiency of dye-sensitized nanocrystalline TiO_2 solar cells: a study by electrical impedance and optical modulation techniques," *Journal of Physical Chemistry B*, vol. 104, no. 9, pp. 2044–2052, 2000.

[6] A. Kongkanand, R. M. Domínguez, and P. V. Kamat, "Single wall carbon nanotube scaffolds for photoelectrochemical solar cells. Capture and transport of photogenerated electrons," *Nano Letters*, vol. 7, no. 3, pp. 676–680, 2007.

[7] W. Wang, P. Serp, P. Kalck, and J. L. Faria, "Photocatalytic degradation of phenol on MWNT and titania composite catalysts prepared by a modified sol-gel method," *Applied Catalysis B: Environmental*, vol. 56, no. 4, pp. 305–312, 2005.

[8] A. J. Miller, R. A. Hatton, and S. R. P. Silva, "Interpenetrating multiwall carbon nanotube electrodes for organic solar cells," *Applied Physics Letters*, vol. 89, no. 13, Article ID 133117, 2006.

[9] A. J. Miller, R. A. Hatton, G. Y. Chen, and S. R. P. Silva, "Carbon nanotubes grown on In_2O_3: Sn glass as large area electrodes for organic photovoltaics," *Applied Physics Letters*, vol. 90, no. 2, Article ID 023105, 2007.

[10] S.-R. Jang, R. Vittal, and K.-J. Kim, "Incorporation of functionalized single-wall carbon nanotubes in dye-sensitized TiO_2 solar cells," *Langmuir*, vol. 20, no. 22, pp. 9807–9810, 2004.

[11] T. Y. Lee, P. S. Alegaonkar, and J.-B. Yoo, "Fabrication of dye sensitized solar cell using TiO_2 coated carbon nanotubes," *Thin Solid Films*, vol. 515, no. 12, pp. 5131–5135, 2007.

[12] W. Wang, P. Serp, P. Kalck, and J. L. Faria, "Visible light photodegradation of phenol on MWNT-TiO_2 composite catalysts prepared by a modified sol-gel method," *Journal of Molecular Catalysis A: Chemical*, vol. 235, no. 1-2, pp. 194–199, 2005.

[13] J. Bisquert, "Chemical capacitance of nanostructured semiconductors: its origin and significance for nanocomposite solar cells," *Physical Chemistry Chemical Physics*, vol. 5, no. 24, pp. 5360–5364, 2003.

[14] R. Kern, R. Sastrawan, J. Ferber, R. Stangl, and J. Luther, "Modeling and interpretation of electrical impedance spectra of dye solar cells operated under open-circuit conditions," *Electrochimica Acta*, vol. 47, no. 26, pp. 4213–4225, 2002.

[15] J. C. Yu and L. Zhang, "Direct sonochemical preparation and characterization of highly active mesoporous TiO_2 with a bicrystalline framework," *Chemistry of Materials*, vol. 14, no. 11, pp. 4647–4653, 2002.

[16] J. Xi, N. A. Dahoudi, Q. Zhang, Y. Sun, and G. Cao, "Effect of annealing temperature on the performances and electrochemical properties of TiO_2 dye-sensitized solar cells," *Science of Advanced Materials*, vol. 4, no. 7, pp. 727–733, 2012.

[17] M. C. Kao, "Effect of annealing temperature of TiO_2 thin films for application in dye-sensitized solar cell," *Hsiuping Journal*, vol. 125, p. 134, 2011.

[18] S.-W. Lee and W. M. Sigmund, "Formation of anatase TiO_2 nanoparticles on carbon nanotubes," *Chemical Communications*, vol. 9, no. 6, pp. 780–781, 2003.

[19] Y. Yu, J. C. Yu, J. G. Yu et al., "Enhancement of photocatalytic activity of mesoporous TiO_2 by using carbon nanotubes," *Applied Catalysis A: General*, vol. 289, p. 186, 2005.

[20] H. Abdullah, N. P. Ariyanto, S. Shaari, B. Yuliarto, and S. Junaidi, "Study of porous nanoflake ZnO for dye-sensitized solar cell application," *The American Journal of Engineering and Applied Sciences*, vol. 21, p. 236, 2009.

[21] B. D. Cullity and S. R. Stock, *Elements of X-Ray Diffraction*, Prentice Hall, 3rd edition, 2001.

[22] S. Nakade, Y. Saito, W. Kubo et al., "Enhancement of electron transport in nano-porous TiO_2 electrodes by dye adsorption," *Electrochemistry Communications*, vol. 5, no. 9, pp. 804–808, 2003.

[23] Y. H. Jung, K.-H. Park, J. S. Oh, D.-H. Kim, and C. K. Hong, "Effect of TiO_2 rutile nanorods on the photoelectrodes of dye-sensitized solar cells," *Nanoscale Research Letters*, vol. 8, no. 1, pp. 1–6, 2013.

[24] Y. Yu, L.-L. Ma, W.-Y. Huang et al., "Sonication assisted deposition of Cu_2O nanoparticles on multiwall carbon nanotubes with polyol process," *Carbon*, vol. 43, no. 3, pp. 670–673, 2005.

[25] E. R. Morales, N. R. Mathews, D. Reyes-Coronado et al., "Physical properties of the CNT: TiO_2 thin films prepared by sol-gel dip coating," *Solar Energy*, vol. 86, no. 4, pp. 1037–1044, 2012.

[26] N. P. Ariyanto, H. Abdullah, and N. S. A. Ghani, "Surface morphology characterisation of Sn-doped ZnO films for antireflective coating," *Materials Research Innovations*, vol. 13, no. 3, pp. 157–160, 2009.

[27] N. P. Ariyanto, H. Abdullah, J. Syarif, B. Yuliarto, and S. Shaari, "Fabrication of zinc oxide-based dye-sensitized solar cell by chemical bath deposition," *Functional Materials Letters*, vol. 3, no. 4, pp. 303–307, 2010.

[28] Y. Lee and M. Kang, "The optical properties of nanoporous structured titanium dioxide and the photovoltaic efficiency on DSSC," *Materials Chemistry and Physics*, vol. 122, no. 1, pp. 284–289, 2010.

[29] H. Abdullah, M. Z. Razali, and M. A. Yarmo, "Preparation of titanium dioxide paste for dye sensitized solar cells (DSSCs)," *Advanced Materials Research*, vol. 139-141, pp. 153–156, 2010.

[30] J. Yu, T. Ma, and S. Liu, "Enhanced photocatalytic activity of mesoporous TiO_2 aggregates by embedding carbon nanotubes as electron-transfer channel," *Physical Chemistry Chemical Physics*, vol. 13, no. 8, pp. 3491–3501, 2011.

[31] K. M. Lee, C. W. Hu, H. W. Chen, and K. C. Ho, "Incorporating carbon nanotube in a low-temperature fabrication process for dye-sensitized TiO_2 solar cells," *Solar Energy Materials and Solar Cells*, vol. 92, no. 12, pp. 1628–1633, 2008.

[32] J. Yu, J. Fan, and B. Cheng, "Dye-sensitized solar cells based on anatase TiO_2 hollow spheres/carbon nanotube composite films," *Journal of Power Sources*, vol. 196, no. 18, pp. 7891–7898, 2011.

[33] V. Dhas, S. Muduli, S. Agarkar et al., "Enhanced DSSC performance with high surface area thin anatase TiO_2 nanoleaves," *Solar Energy*, vol. 85, no. 6, pp. 1213–1219, 2011.

[34] M. Adachi, M. Sakamoto, J. Jiu, Y. Ogata, and S. Isoda, "Determination of parameters of electron transport in dye-sensitized solar cells using electrochemical impedance spectroscopy," *The Journal of Physical Chemistry B*, vol. 110, no. 28, pp. 13872–13880, 2006.

[35] Y. Zhang, J. Zhang, P. Wang et al., "Anatase TiO2 hollow spheres embedded TiO_2 nanocrystalline photoanode for dye-sensitized solar cells," *Materials Chemistry and Physics*, vol. 123, no. 2-3, pp. 595–600, 2010.

[36] A. Mathew, G. M. Rao, and N. Munichandraiah, "Effect of TiO_2 electrode thickness on photovoltaic properties of dye sensitized solar cell based on randomly oriented Titania nanotubes," *Materials Chemistry and Physics*, vol. 127, no. 1-2, pp. 95–101, 2011.

[37] M. Liberatore, F. Decker, L. Burtone et al., "Using EIS for diagnosis of dye-sensitized solar cells performance," *Journal of Applied Electrochemistry*, vol. 39, no. 11, pp. 2291–2295, 2009.